Formation and transformation of schwertmannite through direct Fe 3+ hydrolysis under various geochemical conditions

Hong Ying, Xionghan Feng, Mengqiang Zhu, Bruno Lanson, Fan Liu, Xiaoming Wang

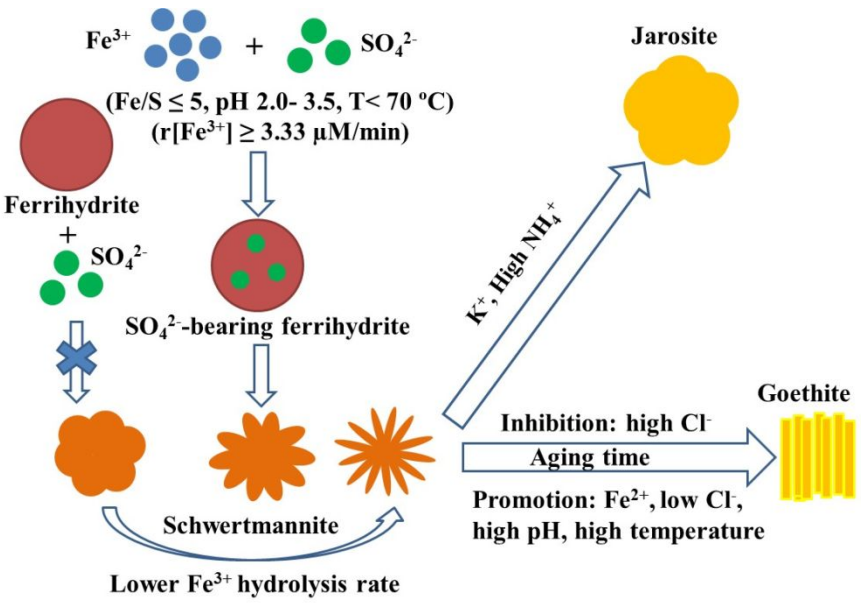

TOC figure

Formation and transformation of schwertmannite through direct Fe^{3+} hydrolysis were systematically explored under various geochemical conditions.

Formation and transformation of schwertmannite through direct Fe^{3+} hydrolysis under various geochemical conditions

Hong Ying[a], Xionghan Feng[a], Mengqiang Zhu[b], Bruno Lanson[c], Fan Liu[a], Xiaoming Wang[a,*]

[a] Key Laboratory of Arable Land Conservation (Middle and Lower Reaches of Yangtze River), Ministry of Agriculture and Rural Affairs, College of Resources and Environment, Huazhong Agricultural University, Wuhan 430070, China

[b] Department of Ecosystem Science and Management, University of Wyoming, Laramie, WY, 82071

[c] Univ. Grenoble Alpes, Univ. Savoie-Mont Blanc, CNRS, IRD, IFSTTAR, ISTerre, F-38000 Grenoble, France

Manuscript includes 1 table and 11 figures.

*Corresponding author:
Xiaoming Wang, Tel: +86 27 87280271; Fax: +86 27 87288618; E-mail: wangxm338@mail.hzau.edu.cn

Electronic supplementary information (ESI) is available free of charge via the internet at http://pubs.rsc.org, including (1) specific experimental conditions of the formation and transformation of schwertmannite; (2) FTIR spectra of schwertmannite obtained from Fe^{3+} hydrolysis-dialysis pathway and of the aging products of schwertmannite formed through Fe^{3+} hydrolysis by adding NaOH; (3) XRD patterns of schwertmannite with the coexistence of K^+ or NH_4^+ and the finial aging products of schwertmannite in the presence of NH_4^+; and (4) schwertmannite transformation rate indicated by Fe_o/Fe_t obtained from acidic dissolution experiments.

Formation and transformation of schwertmannite through direct Fe^{3+} hydrolysis under various geochemical conditions

Abstract

Schwertmannite formation and transformation, key processes that influence the speciation, mobility, and environmental fate of associated trace elements in acid mine drainage (AMD), are primarily studied through Fe^{2+} oxidation. Direct Fe^{3+} hydrolysis is another important schwertmannite formation pathway, but the effects of geochemical conditions on the mineralogical properties of schwertmannite formed via such pathway are poorly known. Here, the formation of schwertmannite through direct Fe^{3+} hydrolysis enforced by heating or adding NaOH and subsequent transformation were systematically examined under various geochemical conditions. Pure schwertmannite is obtained through Fe^{3+} hydrolysis at 25 - 60 °C for 12 mins and subsequent dialysis for 1- 15 days, while minor goethite appear at higher hydrolysis temperatures. Shorter dialysis time and the presence of K^+ or NH_4^+ both slightly increase schwertmannite crystallinity. During Fe^{3+} hydrolysis by adding NaOH, sulfate-bearing ferrihydrite initially forms and then quickly transforms to schwertmannite. In contrast, pre-formed ferrihydrite does not transform to schwertmannite under the same solution conditions, despite sulfate adsorption. Schwertmannite crystallinity slightly increases with decreasing Fe^{3+} hydrolysis rate, and its morphology of "network" structure becomes larger and less dense. As to schwertmannite transformation, high temperature, high pH, and the presence of Fe^{2+} favor its transformation to goethite, while a low Fe^{3+} hydrolysis rate and high concentration of Cl^- hinder the transformation. In contrast, the

presence of K^+ or high NH_4^+ concentration favors schwertmannite transformation to jarosite with the former more readily. These new insights into schwertmannite formation and transformation are essential for predicting the environmental fates of associated trace elements in AMD environments.

Keyword: schwertmannite; Fe^{3+} hydrolysis; formation; transformation; AMD

1. Introduction

Acid mine drainage (AMD, pH < 5) is mainly generated from mining activities of coal and metal sulfide minerals and subsequent waste oxidative weathering, threatening the surrounding environmental quality and ecosystem equilibrium due to its low pH conditions and high concentrations of various metallic contaminants.[1-3] AMD is usually enriched in ferrous (Fe^{2+}) and ferric (Fe^{3+}) ions, sulfate (SO_4^{2-}), and many other cations and anions, resulting in the formation of secondary iron (Fe) minerals with various ions adsorbed on their surface and/or accumulated in their structure.[4-8] Schwertmannite is one of the most common Fe minerals in AMD, with an optimal formation pH of 2.8 - 4.5 and a variable chemical composition described as $Fe_8O_8(OH)_{8-2x}(SO_4)_x \cdot nH_2O$ ($1 \leq x \leq 1.75$).[3, 9-12] Due to its high specific surface area and tunnel structure, schwertmannite is considered as an important sink for trace elements such as As, Se, and Cr, and its formation and transformation thus affect and control the speciation, migration, and environmental fate of these elements in AMD environments.[13-19]

Schwertmannite formation commonly occurs through two pathways depending on the iron sources, *i.e.*, oxidation of Fe^{2+} via biotic and abiotic processes and direct Fe^{3+} hydrolysis.[11, 15, 20-22] In AMD systems, it was reported that schwertmannite is mainly

formed from biotic oxidation of Fe^{2+},[7, 9, 23, 24] hence the schwertmannite formation is primarily studied in laboratory through Fe^{2+} oxidation mediated by microbes or strong chemical oxidants, and subsequent Fe^{3+} hydrolysis-precipitation.[3, 21, 23, 25, 26] However, in AMD affected areas, whether schwertmannite forms through Fe^{2+} oxidation or direct Fe^{3+} hydrolysis depends on the specific solution pH and redox potential of the waters.[27, 28] Additionally, AMD often contains a mixture of Fe^{2+} and Fe^{3+},[29] and the regeneration of Fe^{3+} is a key process to promote the oxidation of sulfide minerals and the formation of secondary iron oxides.[29, 30] Therefore, direct Fe^{3+} hydrolysis can be an important schwertmannite formation pathway, especially when AMD solution contacts surface water or infiltrates soils. However, the formation of schwertmannite through direct Fe^{3+} hydrolysis under various geochemical conditions has not been systematically investigated.

Results of a limited number of studies about the formation of schwertmannite through Fe^{3+} hydrolysis are summarized as follows. The common synthesis of schwertmannite implies Fe^{3+} hydrolysis at 60 ºC and subsequent dialysis for 30 d (hereafter referred to as Fe^{3+} hydrolysis-dialysis),[3] but the influence of Fe^{3+} hydrolysis temperature, dialysis time, and coexistence of ions on the formation of schwertmannite is lacking. In addition to Fe^{3+} hydrolysis-dialysis, Loan et al.[31] examined the formation of schwertmannite by directly mixing acidified $Fe_2(SO_4)_3$ solutions with NaOH at 85 ºC, indicating that low degree of Fe^{3+} supersaturation results in the formation of schwertmannite that possibly nucleates on two-line ferrihydrite aggregates. Studies also showed that schwertmannite formation from direct Fe^{3+} hydrolysis can occur at room

temperature (RT),[32-34] with ferrihydrite-like molecular clusters as intermediate product.[34] The presence of As(V) can inhibit schwertmannite formation.[35] Overall, it remains elusive regarding how Fe^{3+} hydrolysis rate, sulfate concentration, pH, and types of coexisting ions affect schwertmannite formation from Fe^{3+} hydrolysis by adding a base.

Schwertmannite can transform to various Fe-bearing minerals in response to changes in solution conditions. The transformation of schwertmannite is affected by many factors, such as temperature, pH, and types and concentrations of coexisting ions, as well as the formation conditions of pre-formed schwertmannite.[36-43] Under AMD conditions, schwertmannite gradually transforms to jarosite or goethite through a dissolution-recrystallization process.[36, 37, 42] Schwertmannite can also transform to mackinawite or siderite under reducing conditions[44, 45] and to a mixture of lepidocrocite and goethite in the presence of Fe^{2+} at pH 6 and anoxic conditions.[22] The schwertmannite used to study its transformation is mostly synthesized through Fe^{2+} oxidation. However, the physicochemical properties of schwertmannite formed via Fe^{2+} oxidation and Fe^{3+} hydrolysis exhibit significant differences, such as crystal-growth time, morphologies, electro-kinetic properties, etc.[46] Such differences may lead to different behaviors on the transformation of schwertmannite synthesized using the two pathways, which, however, remains unknown.

The objectives of this study are, therefore, to reveal the formation and transformation processes and properties of schwertmannite formed through direct Fe^{3+} hydrolysis under various geochemical conditions. The effects of hydrolysis temperature,

pH, Fe/S ratio (*i.e.*, sulfate concentration), and Fe^{3+} hydrolysis rate on schwertmannite formation and transformation were investigated. The effects of coexisting ions, including Fe^{2+}, Cl^-, K^+, and NH_4^+, were also considered because they might significantly affect the mineralogical properties of schwertmannite and commonly occur in AMD environments.[47-49] The concentrations of dissolved Fe^{3+} and SO_4^{2-} during schwertmannite transformation were determined, and the intermediate and final products were characterized by conventional and synchrotron-based X-ray diffraction (SXRD), Fourier transform infrared spectroscopy (FTIR), high-resolution scanning electron microscopy (SEM), and acidic dissolution experiments.

2. Materials and methods

2.1 Fe^{3+} hydrolysis pathways and the geochemical conditions used for schwertmannite formation and transformation

Schwertmannite formation through direct Fe^{3+} hydrolysis includes two pathways: Fe^{3+} hydrolysis at a certain temperature and subsequent dialysis for some days (*i.e.*, Fe^{3+} hydrolysis-dialysis), and Fe^{3+} hydrolysis by adding NaOH. For the Fe^{3+} hydrolysis-dialysis pathway, influence of hydrolysis temperature, dialysis time, and coexistence of K^+ or NH_4^+ on schwertmannite formation were examined. As to the pathway with Fe^{3+} hydrolysis by adding NaOH, the effects of Fe^{3+} hydrolysis rate, pH, Fe/S molar ratio, and coexistence of Cl^-, K^+, or NH_4^+ on schwertmannite formation were investigated. The effects of these factors, as well as aging temperature and the presence of Fe^{2+} were determined on schwertmannite transformation.

2.2 Effects of hydrolysis temperature, dialysis time, and coexistence of K^+ or NH_4^+

on schwertmannite formation through Fe^{3+} hydrolysis-dialysis

Synthesis of schwertmannite via Fe^{3+} hydrolysis-dialysis was conducted at 60 °C. [3] Briefly, 5.4 g $FeCl_3 \cdot 6H_2O$ and 1.5 g Na_2SO_4 were added into 1 L of deionized water preheated to 60 ºC, and the obtained suspension was then stirred at 60 ºC for an additional 12 mins. The suspension was subsequently cooled to RT and dialyzed for 7 d with a final conductivity < 20 $\mu S \cdot cm^{-1}$. Finally, the suspension was centrifuged, freeze-dried, ground, and stored at 4 °C before being characterized by XRD, SEM, and FTIR. To investigate the hydrolysis temperature effect, similar experiments were performed at 25 ºC, 40 ºC, 50 ºC, 70 ºC, and 80 ºC. In addition, the influence of dialysis time (1, 3, 7, 10, and 15 d with hydrolysis temperatures of 25 °C and 60 °C) and of the additional presence of K^+ or NH_4^+ (hydrolysis temperature of 60 °C and dialysis time of 7 d) on schwertmannite formation were also investigated. The initial molar ratio of Fe/S (Fe/S = 2) was the same in all experiments. All reaction conditions for the formation and transformation of schwertmannite were summarized in Table S1.

The S and Fe contents in the final dried products were measured by dissolving 10 mg solids in 10 mL of 0.2 M acidic ammonium oxalate solution [$(NH_4)_2C_2O_4$, pH 3].[50] The concentrations of Fe and SO_4^{2-} in the solution were determined using the modified 1, 10-phenanthroline colorimetric method[51] and ion chromatography (Dionex ICS-1100), respectively.

2.3 Formation and transformation of schwertmannite through Fe^{3+} hydrolysis by adding NaOH in simulated AMD environments

AMD is acidic (usually pH 2 - 3.5) and enriched in ferrous (Fe^{2+}) and ferric (Fe^{3+})

ions with total Fe and SO_4^{2-} concentrations, respectively, ranging from 500 - 4500 $mg \cdot L^{-1}$ and from 2000 - 6000 $mg \cdot L^{-1}$.[7] Thus, to simulate AMD environments, the pH and dissolved Fe^{3+} and SO_4^{2-} concentrations used in this study were largely varied in these ranges.

2.3.1 Initial phase evolution during Fe^{3+} hydrolysis

To determine the initial phase evolution during Fe^{3+} hydrolysis, 2 mL of 0.8 M NaOH was rapidly mixed with an equal volume of 0.4 M $Fe_2(SO_4)_3$ in a 10 mL tube (OH^-/Fe^{3+} = 1, Fe/S = 0.67, ~pH 2.5). The mixed solution was hydrolyzed at 25 °C for different durations (3.2, 8.7, 45, 50, 59, 70, and 140 min) in different tubes. The obtained suspensions were washed with deionized water, air dried, ground, stored at 4 °C, and then analyzed by SXRD and pair distribution functions (PDF) at beamline 11-ID-B at the Advanced Photon Source (APS).

To further clarify the effects of SO_4^{2-} distribution on the transformation of ferrihydrite to schwertmannite, pre-formed ferrihydrite suspension was aged in the presence of SO_4^{2-} under the same solution conditions. Specifically, SO_4^{2-} solution was added to 50 mL of freshly synthesized ferrihydrite suspension, with pH 2.5, Fe/S molar ratio of 0.67 and a finial volume of 200 mL. After that, the ferrihydrite suspension was aged for the same durations (3.2, 8.7, 45, 50, 59, 70, and 140 min) under stirring.

2.3.2 Effects of Fe^{3+} hydrolysis rate on the formation and long-term aging of schwertmannite

126 mL of 0.2 M NaOH was added dropwise to a 74 mL mixed solution containing $Fe(NO_3)_3$ and Na_2SO_4 at addition rates of 0.5, 0.1, and 0.05 mL/min, respectively,

corresponding Fe^{3+} hydrolysis rates of 33.33, 6.67, and 3.33 μM/min. The direct mix of NaOH, $Fe(NO_3)_3$ and Na_2SO_4 solutions was recognized as control system (named as mixed directly), approximately representing an infinite Fe^{3+} hydrolysis rate. Solution pH was then adjusted to 3 for all experiments with a Fe/S molar ratio of 2 [$c(Fe^{3+})$ = 48.55 mM, $c(SO_4^{2-})$ = 24.275 mM]. In addition, to determine the effects of Fe^{2+} on schwertmannite transformation, a Fe^{2+} solution [$c(Fe^{3+})/c(Fe^{2+})$ = 10] was added to the fresh schwertmannite suspension formed form the condition of a NaOH addition rate of 0.1 mL/min. Subsequently, all samples were sealed and aged at 60 °C for 96 h, during which, the solution pH were maintained at pH 3 by adding 0.1 M NaOH or HNO_3 at regular time intervals. The containers were open to air during pH adjustment and sampling, allowing entrance of atmospheric O_2 to the reaction systems. At pre-set time intervals, a 15 mL suspension was sampled and passed through a 0.22 μm membrane filter mounted on a vacuum apparatus. The dissolved SO_4^{2-} and Fe concentrations in the filtrates were measured as described above, whereas the wet solids on the membrane were rinsed with 30 mL deionized water, air dried, ground, and analyzed by XRD, FTIR, SEM, and acidic dissolution.

2.3.3 Effects of pH, Fe/S molar ratio, and temperature on the long-term aging of schwertmannite

Solutions containing $Fe(NO_3)_3$ and Na_2SO_4 with Fe/S molar ratios of 1.5, 2.0, 2.5, 5.0, 8.0 or 10.0 [$c(Fe^{3+})$ = 48.55 mM] were directly mixed with different amounts of 0.2 M NaOH solution, leading to final pH values of pH 2.0, 2.5, 3.0 and 3.5 with total suspension volume of 200 mL. The suspensions with different pHs (Fe/S molar ratio =

2.0) were aged at 80 °C for 96 h, while the suspensions with different Fe/S molar ratios (pH = 3.0) were aged at 60 °C for 96 h. Subsequent experimental details are the same as in Section 2.3.2.

2.3.4 Effects of co-existing Cl^-, K^+, or NH_4^+ on the long-term aging of schwertmannite

Solutions containing $Fe(NO_3)_3$, Na_2SO_4, and NaCl [$c(Fe^{3+})$ = 48.55 mM, Fe/S = 2, Fe/Cl = 2, 0.2] were directly mixed with 0.2 M NaOH solution to obtain schwertmannite suspensions with a total volume of 200 mL. The schwertmannite suspensions were then aged at 60 °C and pH 3 for 96 h. In addition, solutions containing $Fe(NO_3)_3$, K_2SO_4 or $(NH_4)_2SO_4$ [$c(Fe^{3+})$ = 48.55 mM, Fe/S = 2 and 0.2, Fe/K^+ or NH_4^+=1 and 0.1] were directly mixed with 0.2 M NaOH solution to obtain schwertmannite suspensions. The suspensions were subsequently aged at 80 °C and pH 2 for 96 h. Subsequent experimental details are the same as in Section 2.3.2.

2.3.5 Acidic dissolution experiments

To explore the transformation rate of schwertmannite under different conditions, 10 mg of dried intermediate samples were dissolved in 10 mL of 0.2 M acidic ammonium oxalate solution (pH 3, Fe_o) or 4 M HCl solution (Fe_t) at RT for 2 h under stirring. Resulting solution was then immediately filtered through a 0.22 μm membrane. The Fe concentration in the solution was measured using a modified 1, 10-phenanthroline colorimetric method.[51] The ratio of Fe_o/Fe_t indicates the transformation rate of schwertmannite.

2.4 Solid characterizations

Conventional XRD patterns for phase identification were recorded from 10 to 70° at a scan speed of 1°·min^{-1} on a Bruker D8 Advance X-ray diffractometer equipped with a LynxEye detector using Ni-filtered Cu Kα radiation (λ = 0.15418 nm). To identify mineral phases with poor crystallinity, synchrotron-based XRD data of part samples were collected at beamline BL14B1 (λ = 0.6895 Å, scanning from 0.5 to 30° and exposure time of 30 s) at the Shanghai Synchrotron Radiation Facility (SSRF) [52] or at beamline 11-ID-B at the Advanced Photon Source (APS), Argonne National Laboratory (X-ray energy of 58.86 keV, λ = 0.2112 Å).[50]

The morphology and particle size of the samples were observed by SEM (SU8000) at an accelerating voltage of 10 or 20 kV. Specifically, a small amount of sample was pasted on conductive glue, and then plated using a sputtering apparatus. In addition, FTIR of the samples was recorded on a Bruker VERTEX 70 spectrophotometer. The samples were mixed gently with KBr (~1% sample weight) in an agate mortar and pelletized. Each sample was collected 128 scans with a resolution of 4 cm^{-1} over the 4000–400 cm^{-1} against the air background.

3. Results and discussion

3.1 Formation of schwertmannite through Fe^{3+} hydrolysis-dialysis

XRD patterns of the products obtained from different Fe^{3+} hydrolysis temperatures are shown in Figure 1a. With increasing hydrolysis temperature from 25 - 60 °C, pure schwertmannite is obtained, and its crystallinity gradually increases evidenced by the enhanced peak intensity at 2.55 Å (Fig. 1a). As shown in Table 1, a higher hydrolysis temperature (25 - 60 °C) leads to a higher SO_4^{2-} content and a lower Fe/S ratio,

suggesting that schwertmannite crystallinity might be related to the sulfate content,[3] *i.e.*, a higher sulfate content leads to an increased crystallinity. At 25 °C, schwertmannite is flower-shaped and composed of small thin plates (Fig. 2a). With increasing hydrolysis temperature, the thin plates transform to long strips, connecting to a "sea-urchin"-like structure (Fig. 2a-d). When the hydrolysis temperature increases to 70 °C and above, minor goethite impurities form, evidenced by its characteristic peaks at 4.18 Å and 1.72 Å (Fig. 1a), while the crystallinity of schwertmannite slightly decreases (Fig. 1a). In addition, SO_4^{2-} content decreases and Fe/S ratio increases (Table 1), and the long strips of schwertmannite become more clustered (Fig. 2e-f).

The FTIR spectra of these samples are similar and consistent with typical schwertmannite IR fingerprint.[50, 53] These spectra consist of a broad triply degenerate asymmetric stretching (ν_3) band at ~1125 cm^{-1} with two shoulder bands at ~1050 and ~1205 cm^{-1}, a ν_1 fundamental of the symmetric sulfate stretching at 980 cm^{-1}, a ν_4 bending band at ~610 cm^{-1}, and a Fe-O stretching band at ~698 cm^{-1} (Fig. S1a). Additional weak IR vibration bands at 885 cm^{-1} and 792 cm^{-1} are shown for the samples hydrolyzed at 70 °C and 80 °C, indicating the formation of minor goethite (Fig. S1a), consistent with XRD results (Fig. 1a).

With increasing dialysis time, diffraction peak intensities of schwertmannite slightly decrease, especially for the peak at 2.55 Å (Fig. 1b), consistent with the decrease of SO_4^{2-} content and of sulfate IR band intensities (Table 1 and Fig. S1b). In addition, schwertmannite particles aggregate more closely (Figs. 2g-i), leading to a "hedgehog" morphology.[54] Furthermore, compared to the Na^+ system, the presence of

K^+ or NH_4^+ (Fig. 1c) slightly increases the crystallinity of schwertmannite but decreases the SO_4^{2-} content in schwertmannite (Table 1).

3.2 Mineral evolution during Fe^{3+} hydrolysis by adding NaOH

During Fe^{3+} hydrolysis in the presence of SO_4^{2-}, XRD patterns of the intermediate products indicate that ferrihydrite is the initial product and schwertmannite is observed later but within 45 min (Fig. 3a). The corresponding PDF data [G(r)s] of intermediate products show that the PDF data of initial sample (~3.2 min) is similar to that of a ferrihydrite reference. With increasing aging time, the intensity of Fe-Fe peak at 5.42 Å increases, and the Fe-Fe peaks at 7.40 Å and 11.06 Å and Fe-O peak at 6.08 Å gradually appear and increase, indicative of schwertmannite formation (Fig. 3b). In contrast, the pre-formed two-line ferrihydrite aged in the same sulfate concentration and solution pH does not transform to schwertmannite (Fig. 3c).

Sulfate-bearing ferrihydrite thus appears as an intermediate phase during the formation of schwertmannite (Fig. 3), similar with the observation in Zhu et al.[34]. Transformation from ferrihydrite to schwertmannite is most likely because of a higher thermodynamic stability than ferrihydrite.[31, 54] However, the contrast between the transformation from intermediate ferrihydrite-like mineral (Fig. 3a) and from pre-formed ferrihydrite (Fig. 3c) suggests that sulfate is closely associated with ferrihydrite in a way that differs from simple surface adsorption.[55] This is not unexpected because sulfate and ferrihydrite co-precipitate during Fe^{3+} hydrolysis in the presence of sulfate. The sulfate may be incorporated into the structural defects of ferrihydrite. Such structure may have some similarity to that of schwertmannite [3, 50] and

thus the formed ferrihydrite readily transforms to schwertmannite. In addition, the ferrihydrite formed in the presence of sulfate may have smaller particle size and more structural defects than ferrihydrite synthesized in the absence of sulfate, which further enhances its transformation to schwertmannite.[56]

Schwertmannite can form at 25 °C through both Fe^{3+} hydrolysis-dialysis (Fig. 1) and Fe^{3+} hydrolysis by adding NaOH (Fig. 3, 4a and S2). However, a theoretical calculation indicates that schwertmannite formation through direct Fe^{3+} hydrolysis is not thermodynamically spontaneous under ambient condition (~ 25 °C), due to the reaction free energy $\Delta G°_{298}$ of 6.275 kJ·mol^{-1} as the following equation. [7]

$$Fe^{3+}(aq) + 7/4H_2O(l) + 1/8SO_4^{2-}(aq) = 1/8Fe_8O_8(OH)_6SO_4(s)\ (Sch) + 11/4H^+(aq)$$

This apparent discrepancy could be explained by the migration of protons (H^+) through the dialysis membrane into distilled water during dialysis process. As a result, the solution pH in the dialysis bag, initially very low and unfavorable to Fe^{3+} hydrolysis, gradually increases and then induces schwertmannite formation. On the other hand, the schwertmannite readily forms from Fe^{3+} hydrolysis in the presence of sulfate by adding NaOH at 25 °C (Fig. 3 and 4), consistent with previous reports.[32-34] Consequently, direct Fe^{3+} hydrolysis should be considered as an important pathway of schwertmannite formation in watershed or soils surrounded by AMD with a relative high pH.

3.3 Effects of geochemical conditions on schwertmannite formation through Fe^{3+} hydrolysis by adding NaOH

3.3.1 Effect of Fe^{3+} hydrolysis rate

XRD patterns indicate that pure schwertmannite forms at different Fe^{3+} hydrolysis

rates (above 3.33 μM Fe/min), with a lower hydrolysis rate leading to an improved crystallinity, compared to the mixed directly system (Fig. 4a). In addition, schwertmannite morphology varies substantially with Fe^{3+} hydrolysis rate, exhibiting longer strips and resulting in larger and looser aggregates at a lower Fe^{3+} hydrolysis rate, similar to the sea urchin-like aggregates that form from Fe^{2+} oxidation.[46] However, the morphology obtained from mixed directly system is block agglomerate (Fig. 4b). These schwertmannite samples, obtained from different Fe^{3+} hydrolysis rates, should have distinct surface reactivity and geochemical behaviors, which need to be further studied.

3.3.2 Effects of pH, Fe/S molar ratio and co-existing ions

Schwertmannite can form through Fe^{3+} hydrolysis over the pH range of 2.0 – 3.5 (Fig 4a, 9a and S2) that is slightly wider compared to that of Fe^{2+} oxidation (*i.e.*, pH 2.4 - 3.2 [46]). In addition, schwertmannite can be obtained only at low initial Fe/S molar ratio (Fe/S ≤ 5) (Fig. 3 and 9b), *i.e.*, high sulfate concentration, while ferrihydrite forms when the Fe/S molar ratios exceed 8 to 10, suggesting that sulfate must be present in excess, relative to the ideal mineral composition, to allow for schwertmannite formation.

XRD patterns indicate that the presence of Cl^- does not affect schwertmannite formation (Fig. 9d), suggesting that although Cl^- can promote akaganéite ($FeO(OH)_{1-x}Cl_x$) formation under acidic conditions,[34] the presence of numerous sulfate probably inhibits the formation of akaganéite, similar to the reports in Fe^{2+} bio-oxidation system.[48, 57] Pure schwertmannite could thus be synthesized through $FeCl_3$ hydrolysis-dialysis if sufficient sulfate is present.[3] Additionally, the presence of K^+ or

NH_4^+ slightly increases schwertmannite crystallinity (Fig. S2), similar to the Fe^{3+} hydrolysis-dialysis pathway (Fig. 1c), probably because K^+ or NH_4^+ ions enter the schwertmannite tunnel structure during Fe^{3+} hydrolysis, thus enhancing schwertmannite crystal growth.

3.4 Effects of geochemical conditions on the transformation of schwertmannite formed through Fe^{3+} hydrolysis by adding NaOH

3.4.1 Effect of Fe^{3+} hydrolysis rate

During the transformation of schwertmannite formed at different Fe^{3+} hydrolysis rates, minor goethite form only in the mixed directly sample after a 3 h aging (Fig. 5a). With increasing aging time to 24 h, goethite is present in all samples, with more goethite occurring at higher Fe^{3+} hydrolysis rate (Fig. 5b), suggesting that the schwertmannite obtained at a higher Fe^{3+} hydrolysis rate is less stable, possibly due to its lower crystallinity. FTIR spectra of the samples aged for 3 h (Fig. 5c) and 24 h (Fig. 5d) show that the characteristic Fe-O stretching band of schwertmannite at ~698 cm^{-1} decreases with aging time, whereas the characteristic OH bending vibration bands of goethite at 885 cm^{-1} and 792 cm^{-1} increase with increasing Fe^{3+} hydrolysis rate and aging time, confirming XRD results (Fig. 5a and 5b). Thus, lower Fe^{3+} hydrolysis rate leads to larger crystallite size and higher structural stability of schwertmannite, thus disfavoring its transformation to other phases. This observation was also made for schwertmannite formed from Fe^{2+} oxidation.[15, 20, 58]

3.4.2 Effect of the presence of Fe^{2+}

After aging for 24 h, XRD patterns indicate that goethite diffraction peaks are

stronger if Fe^{2+} is present (Fig. 6a), compared to the Fe^{2+}-free system (Fig 5b), suggesting that Fe^{2+} significantly accelerates schwertmannite transformation to goethite. In addition, the concentration of dissolved SO_4^{2-} is higher in the presence of Fe^{2+} than that in the Fe^{2+}-free system (Fig. 6b), indicating that Fe^{2+} promotes the release of sulfate during schwertmannite dissolution and transformation. During the aging process, the concentration of dissolved Fe^{2+} decreases with increasing aging time, while that of dissolved SO_4^{2-} increases (Fig. 6b), suggesting that schwertmannite transformation to goethite occurs through a dissolution-recrystallization mechanism by consuming Fe^{2+} and releasing SO_4^{2-}. Enhancement of schwertmannite transformation in the presence of Fe^{2+} possibly results from two aspects. On one hand, aqueous Fe(II) species can exchange structural Fe(III), thus enhancing the mineral phase reorganization, as evidenced by stable Fe isotope tracers.[59-61] On the other hand, electron transfer between adsorbed Fe(II) and structural Fe(III) promotes the reductive dissolution of schwertmannite and its subsequent recrystallization.[60, 62, 63]

3.4.3 Effects of pH, temperature, and Fe/S molar ratio

At 80 ºC and Fe/S = 2, the concentration of dissolved Fe^{3+} decreases with increasing pH from 2.0 to 3.5 (Fig. 7a), while that of dissolved SO_4^{2-} increases (Fig. 8a), indicating that a higher pH enhances SO_4^{2-} release and thus the transformation from schwertmannite to goethite. This transformation is supported by the XRD patterns (Fig. 9a) and the lower Fe_o/Fe_t (ratio of dissolved Fe in oxalate to total Fe) measured at higher pH values (Fig. S4b). Additionally, FTIR spectra indicate that the characteristic Fe-O stretching band of schwertmannite at ~701 cm^{-1} gradually decreases whereas OH

bending vibration bands of goethite at 885 cm^{-1} and 792 cm^{-1} increase with increasing pH (Fig. S3a), further confirming the above analyses. The increased transformation rate of schwertmannite to goethite can be partially ascribed to the easier sulfate release at a higher pH.[36]

For a given pH and Fe/S molar ratio, the concentration of dissolved Fe^{3+} substantially decreases with increasing aging temperature (from 25 to 80 °C) and aging time (Fig. 7c). As to dissolved SO_4^{2-}, it increases slightly at 25 °C and more significantly at higher temperatures with increasing aging time (Fig. 8b), suggesting that SO_4^{2-} release is enhanced at a higher temperature during schwertmannite transformation. Additionally, XRD patterns (Fig. 9c and S3c) and acidic dissolution results (Fig. S4a) indicate that goethite formation is favored at higher aging temperatures and longer aging time, consistent with lower concentration of dissolved Fe^{3+} (Fig. 7c) and higher concentration of dissolved SO_4^{2-} (Fig. 8b). In addition, the mineral phases formed at different Fe/S molar ratios exhibit different stabilities at 60 °C and pH 3 (Fig. 9b and S3b), with lower Fe/S molar ratio resulting in lower concentration of dissolved Fe^{3+} (Fig. 8b). As a consequence, schwertmannite obtained at a lower Fe/S molar ratio (Fe/S ≤ 5) transforms more readily to goethite than ferrihydrite which is obtained at higher Fe/S ratios (Fe/S > 5) (Fig. 9b and S3b).

3.4.4 Effects of co-existing Cl^-, K^+, or NH_4^+

Compared to the system without Cl^-, the presence of Cl^- ($Fe/Cl^- = 2$) accelerates the release of SO_4^{2-} (Fig. 8c), possibly because Cl^- promotes SO_4^{2-} release by ligand exchange, enhancing goethite formation (Fig. 9d). In contrast, a high concentration of

Cl^- ($Fe/Cl^- = 0.2$) inhibits SO_4^{2-} release and the transformation of schwertmannite to goethite (Fig. 8c and 9d), possibly because massive Cl^- adsorption on schwertmannite surface impedes SO_4^{2-} release and thus the dissolution-recrystallization process. As reported previously, adsorption of ions on schwertmannite surface could stabilize its structure.[40, 64]

The presence of K^+ promotes hydrolysis and precipitation of dissolved Fe^{3+} (Fig. 7d) and inhibits SO_4^{2-} release (Fig. 8d) through the formation of K^+-bearing jarosite, exhibiting aggregated spherical particle morphology (Fig. 9d and 10d). K^+-bearing jarosite formation is also confirmed by FTIR spectrum with bands at around 1080 ~ 1200 cm^{-1}, 1008 cm^{-1}, and 628 cm^{-1} (Fig. S3d), respectively, assigned to the vibrational modes of $v_3(SO_4^{2-})$, $v_1(SO_4^{2-})$, and $v_4(SO_4^{2-})$.[65] Similarly, a high NH_4^+ concentration ($Fe/NH_4^+ = 0.1$) favors jarosite formation with very low concentration of dissolved SO_4^{2-} (Fig. 8d), leading to the coexistence of goethite and NH_4^+-bearing jarosite (Fig. S5), coincident with the results observed in Fe^{2+} bio-oxidation system.[66, 67] More lath-like particles and looser aggregates are observed at a higher concentration of NH_4^+ (Fig. 10 b). However, the presence of low NH_4^+ ($Fe/NH_4^+ = 1$) increases SO_4^{2-} release (Fig. 8d), thus favoring the formation of goethite (Fig. S5). Compared to NH_4^+, the presence of K^+ is easier to induce jarosite formation, consistent with a previous study indicating that the ability of K^+ to promote jarosite formation is ~ 75× greater than that of NH_4^+,[68] probably because that the ionic radius of hydrated K^+ (1.32 Å) fits better in jarosite structure than that of NH_4^+ (1.44 Å).

4. Conclusion and implications

In the present study, schwertmannite formation through direct Fe^{3+} hydrolysis and its subsequent transformation have been systematically investigated under various geochemical conditions. Schwertmannite can be obtained over a Fe^{3+} hydrolysis temperature range of 25 - 60 °C, a pH range of 2.0 – 3.5, molar ratios of Fe/S lower than 5, Fe^{3+} hydrolysis rates higher than 3.33 μM/min, and in the presence of Cl^-, K^+ or NH_4^+ (Fig. 11). Such an extended range of conditions suggests that direct Fe^{3+} hydrolysis is an important pathway for schwertmannite formation in natural AMD affected environments, and that the chemical composition, micro-structure, and reactivity of schwertmannite vary with these geochemical conditions. Actually, schwertmannite formed through Fe^{2+} oxidation also includes a process of Fe^{3+} hydrolysis-precipitation, and these new insights into schwertmannite formation through direct Fe^{3+} hydrolysis are also essential to understand the mineralization process during Fe^{2+} oxidation in AMD surroundings.

During the schwertmannite formation through direct Fe^{3+} hydrolysis, sulfate-bearing ferrihydrite is an intermediate product and sulfate is likely incorporated into structural defects of ferrihydrite particles, rather than simply adsorbed on their surfaces, to induce schwertmannite formation. Due to the abundance of sulfate in AMD environments, these anions readily co-precipitate with ferrihydrite through Fe^{3+} hydrolysis, allowing for the subsequent transformation to schwertmannite and accounting for the more occurrence of schwertmannite than ferrihydrite in AMD affected areas.

Schwertmannite readily transforms to more stable goethite and jarosite. High

temperature, high pH, and the presence of Fe^{2+} all enhance the transformation to goethite by promoting the release of structural sulfate, whereas a low Fe^{3+} hydrolysis rate and high concentration of Cl^- hinder this transformation. Moreover, the presence of both K^+ and high concentration of NH_4^+ favor schwertmannite transformation to K^+- or NH_4^+-bearing jarosite (Fig. 11). These new insights into schwertmannite formation and transformation under various geochemical conditions are vital to understand the mineralogical properties of schwertmannite and predict the environmental behavior and fate of trace elements associated with schwertmannite in AMD affected environments.

Acknowledgements

This study was supported by the National Natural Science Foundation of China (No. 41601228 and 41977021) and the Fundamental Research Funds for the Central Universities (No. 2662019QD015). The authors thank beamline BL14B1 (Shanghai Synchrotron Radiation Facility) and beamline 11-ID-B at Advanced Photon Source (APS), Argonne National Laboratory (ANL), for providing the beam time and assistance during data collection.

References

1. G. S. Simate and S. Ndlovu, Acid mine drainage: Challenges and opportunities, *J. Environ. Chem. Eng.*, 2014, **2**, 1785-1803.
2. K. K. Kefeni, T. A. M. Msagati and B. B. Mamba, Acid mine drainage: Prevention, treatment options, and resource recovery: A review, *J. Cleaner Prod.*, 2017, **151**, 475-493.
3. J. M. Bigham, U. Schwertmann, L. Carlson and E. Murad, A poorly crystallized oxyhydroxysulfate of iron formed by bacterial oxidation of Fe(II) in acid-mine waters, *Geochim. Cosmochim. Acta*, 1990, **54**, 2743-2758.
4. Y. Xie, G. Lu, C. Yang, L. Qu, M. Chen, C. Guo and Z. Dang, Mineralogical characteristics of sediments and heavy metal mobilization along a river watershed affected by acid mine drainage,

PLoS One, 2018, **13**, e0190010.

5. S. Paikaray, J. Gottlicher and S. Peiffer, Removal of As(III) from acidic waters using schwertmannite: Surface speciation and effect of synthesis pathway, *Chem. Geol.*, 2011, **283**, 134-142.

6. J. Antelo, S. Fiol, D. Gondar, R. Lopez and F. Arce, Comparison of arsenate, chromate and molybdate binding on schwertmannite: Surface adsorption vs anion-exchange, *J. Colloid Interface Sci.*, 2012, **386**, 338-343.

7. L. Zhou, Biomineralization: a pivotal process in developing a novel passive treatment system for acid mine drainage, *Acta Chim. Sin.*, 2017, **75**, 552-559 (in chinese).

8. M. P. Asta, J. Cama, M. Martinez and J. Gimenez, Arsenic removal by goethite and jarosite in acidic conditions and its environmental implications, *J. Hazard. Mater.*, 2009, **171**, 965-972.

9. J. M. Bigham, L. Carlson and E. Murad, Schwertmannite, a new iron oxyhydroxysulphate from pyhasalmi, finland, and other localities, *Mineral. Mag.*, 1994, **58**, 641-648.

10. U. Schwertmann, J. M. Bigham and E. Murad, The 1st occurrence of schwertmannite in a natural stream environment, *Eur. J. Mineral.*, 1995, **7**, 547-552.

11. S. Regenspurg, A. Brand and S. Peiffer, Formation and stability of schwertmannite in acidic mining lakes, *Geochim. Cosmochim. Acta*, 2004, **68**, 1185-1197.

12. A. Fernandez-Martinez, V. Timon, G. Roman-Ross, G. J. Cuello, J. E. Daniels and C. Ayora, The structure of schwertmannite, a nanocrystalline iron oxyhydroxysulfate, *Am. Mineral.*, 2010, **95**, 1312-1322.

13. E. D. Burton, R. T. Bush, S. G. Johnston, K. M. Watling, R. K. Hocking, L. A. Sullivan and G. K. Parker, Sorption of arsenic(V) and arsenic(III) to schwertmannite, *Environ. Sci. Technol.*, 2009, **43**, 9202-9207.

14. S. Carrero, A. Fernandez-Martinez, R. Perez-Lopez, A. Poulain, E. Salas-Colera and J. M. Nieto, Arsenate and selenate scavenging by basaluminite: Insights into the reactivity of aluminum phases in acid mine drainage, *Environ. Sci. Technol.*, 2017, **51**, 28-37.

15. Z. Zhang, G. Guo, X. Li, Q. Zhao, X. Bi, K. Wu and H. Chen, Effects of hydrogen-peroxide supply rate on schwertmannite microstructure and chromium(VI) adsorption performance, *J. Hazard. Mater.*, 2018, **367**, 520-528.

16. P. Acero, C. Ayora, C. Torrento and J. M. Nieto, The behavior of trace elements during schwertmannite precipitation and subsequent transformation into goethite and jarosite, *Geochim. Cosmochim. Acta*, 2006, **70**, 4130-4139.

17. J. Antelo, S. Fiol, D. Gondar, C. Perez, R. Lopez and F. Arce, Cu(II) incorporation to schwertmannite: Effect on stability and reactivity under AMD conditions, *Geochim. Cosmochim. Acta*, 2013, **119**, 149-163.

18. C. Fan, C. Guo, Y. Zeng, Z. Tu, Y. Ji, J. R. Reinfelder, M. Chen, W. Huang, G. Lu, X. Yi and Z. Dang, The behavior of chromium and arsenic associated with redox transformation of schwertmannite in AMD environment, *Chemosphere*, 2019, **222**, 945-953.

19. P. Cruz-Hernández, R. Pérez-López, A. Parviainen, M. B. J. Lindsay and J. M. Nieto, Trace element-mineral associations in modern and ancient iron terraces in acid drainage environments, *Catena*, 2016, **147**, 386-393.

20. J. Song, S. Y. Jia, H. T. Ren, S. H. Wu and X. Han, Application of a high-surface-area schwertmannite in the removal of arsenate and arsenite, *Int. J. Environ. Sci. Technol.*, 2014, **12**, 1559-1568.

21. Y. Liao, L. Zhou, S. Bai, J. Liang and S. Wang, Occurrence of biogenic schwertmannite in

sludge bioleaching environments and its adverse effect on solubilization of sludge-borne metals, *Appl. Geochem.*, 2009, **24**, 1739-1746.

22. L. Liu, Z. Jia, W. Tan, S. L. Suib, L. Ge, G. Qiu and R. Hu, Abiotic photomineralization and transformation of iron oxide nanominerals in aqueous systems, *Environ. Sci.: Nano*, 2018, **5**, 1169-1178.
23. M. Kawano and K. Tomita, Geochemical modeling of bacterially induced mineralization of schwertmannite and jarosite in sulfuric acid spring water, *Am. Mineral.*, 2001, **86**, 1156-1165.
24. W. Stumm and J. J. Morgan, *Aquatic chemistry: an introduction emphasizing chemical equilibria in natural waters.*, 1970.
25. Y. Liao, L. Zhou, J. Liang and H. Xiong, Biosynthesis of schwertmannite by Acidithiobacillus ferrooxidans cell suspensions under different pH condition, *Mater. Sci. Eng., C*, 2009, **29**, 211-215.
26. J. S. Tischler, C. Wiacek, E. Janneck and M. Schlomann, Microbial abundance in the schwertmannite formed in a mine water treatment plant, *Mine Water Environ.*, 2013, **32**, 258-265.
27. D. K. Nordstrom, Hydrogeochemical processes governing the origin, transport and fate of major and trace elements from mine wastes and mineralized rock to surface waters, *Appl. Geochem.*, 2011, **26**, 1777-1791.
28. S. Carrero, R. Pérez-López, A. Fernandez-Martinez, P. Cruz-Hernández, C. Ayora and A. Poulain, The potential role of aluminium hydroxysulphates in the removal of contaminants in acid mine drainage, *Chem. Geol.*, 2015, **417**, 414-423.
29. J. G. Skousen, A. Sexstone and P. F. Ziemkiewicz, West Virginia University and the National Mine Land Reclamation Center, Morgantown, 1996, ch. 6.
30. D. K. Nordstrom, D. W. Blowes and C. J. Ptacek, Hydrogeochemistry and microbiology of mine drainage: An update, *Appl. Geochem.*, 2015, **57**, 3-16.
31. M. Loan, W. R. Richmond and G. M. Parkinson, On the crystal growth of nanoscale schwertmannite, *J. Cryst. Growth*, 2005, **275**, E1875-E1881.
32. W. D. Burgos, T. Borch, L. D. Troyer, F. B. Luan, L. N. Larson, J. F. Brown, J. Lambson and M. Shimizu, Schwertmannite and Fe oxides formed by biological low-pH Fe(II) oxidation versus abiotic neutralization: Impact on trace metal sequestration, *Geochim. Cosmochim. Acta*, 2012, **76**, 29-44.
33. L. Reichelt and M. Bertau, Transformation of nanostructured schwertmannite and 2-line-ferrihydrite into hematite, *Z. Anorg. Allg. Chem.*, 2015, **641**, 1696-1700.
34. M. Zhu, B. Legg, H. Zhang, B. Gilbert, Y. Ren, J. F. Banfield and G. A. Waychunas, Early stage formation of iron oxyhydroxides during neutralization of simulated acid mine drainage solutions, *Environ. Sci. Technol.*, 2012, **46**, 8140-8147.
35. P. Cruz-Hernández, S. Carrero, R. Pérez-López, A. Fernandez-Martinez, M. B. J. Lindsay, C. Dejoie and J. M. Nieto, Influence of As(V) on precipitation and transformation of schwertmannite in acid mine drainage-impacted waters, *Eur. J. Mineral.*, 2019, **31**, 237-245.
36. J. Jonsson, P. Persson, S. Sjoberg and L. Lovgren, Schwertmannite precipitated from acid mine drainage: phase transformation, sulphate release and surface properties, *Appl. Geochem.*, 2005, **20**, 179-191.
37. U. Schwertmann and L. Carlson, The pH-dependent transformation of schwertmannite to goethite at 25 °C, *Clay Miner.*, 2005, **40**, 63-66.
38. K. H. Knorr and C. Blodau, Controls on schwertmannite transformation rates and products, *Appl.*

Geochem., 2007, **22**, 2006-2015.

39. L. E. Davidson, S. Shaw and L. G. Benning, The kinetics and mechanisms of schwertmannite transformation to goethite and hematite under alkaline conditions, *Am. Mineral.*, 2008, **93**, 1326-1337.

40. E. D. Burton, S. G. Johnston, K. Watling, R. T. Bush, A. F. Keene and L. A. Sullivan, Arsenic effects and behavior in association with the Fe(II)-catalyzed transformation of schwertmannite, *Environ. Sci. Technol.*, 2010, **44**, 2016-2021.

41. E. D. Burton and S. G. Johnston, Impact of silica on the reductive transformation of schwertmannite and the mobilization of arsenic, *Geochim. Cosmochim. Acta*, 2012, **96**, 134-153.

42. J. Sanchez-Espana, I. Yusta and G. A. Lopez, Schwertmannite to jarosite conversion in the water column of an acidic mine pit lake, *Mineral. Mag.*, 2012, **76**, 2659-2682.

43. S. Paikaray and S. Peiffer, Dissolution kinetics of sulfate from schwertmannite under variable pH conditions, *Mine Water Environ.*, 2010, **29**, 263-269.

44. E. D. Burton, R. T. Bush, L. A. Sullivan and D. R. G. Mitchell, Reductive transformation of iron and sulfur in schwertmannite-rich accumulations associated with acidified coastal lowlands, *Geochim. Cosmochim. Acta*, 2007, **71**, 4456-4473.

45. S. G. Johnston, E. D. Burton and E. M. Moon, Arsenic Mobilization Is Enhanced by Thermal Transformation of Schwertmannite, *Environ. Sci. Technol.*, 2016, **50**, 8010-8019.

46. Z. Zhang, X. Bi, X. Li, Q. Zhao and H. Chen, Schwertmannite: occurrence, properties, synthesis and application in environmental remediation, *RSC Adv.*, 2018, **8**, 33583-33599.

47. H. M. Wang, J. M. Bigham and O. H. Tuovinen, Formation of schwertmannite and its transformation to jarosite in the presence of acidophilic iron-oxidizing microorganisms, *Mater. Sci. Eng., C*, 2006, **26**, 588-592.

48. H. Xiong, Y. Liao and L. Zhou, Influence of chloride and sulfate on formation of akaganéite and schwertmannite through ferrous biooxidation by acidithiobacillus ferrooxidans cells, *Environ. Sci. Technol.*, 2008, **42**, 8681-8686.

49. S. Paikaray, C. Schröder and S. Peiffer, Schwertmannite stability in anoxic Fe(II)-rich aqueous solution, *Geochim. Cosmochim. Acta*, 2017, **217**, 292-305.

50. X. Wang, C. Gu, X. Feng and M. Zhu, Sulfate local coordination environment in schwertmannite, *Environ. Sci. Technol.*, 2015, **49**, 10440-10448.

51. E. D. Burton, R. T. Bush, L. A. Sullivan and D. R. G. Mitchell, Schwertmannite transformation to goethite via the Fe(II) pathway: Reaction rates and implications for iron-sulfide formation, *Geochim. Cosmochim. Acta*, 2008, **72**, 4551-4564.

52. T. Yang, W. Wen, G. Yin, X. Li, M. Gao, Y. Gu, L. Li, Y. Liu, H. Liu, X. Zhang, B. Zhao, T. Liu, Y. Yang, Z. Li, X. Zhou and X. Gao, Introduction of the X-ray diffraction beamline of SSRF, *Nucl. Sci. Tech.*, 2015, **26**, 020101.

53. J. F. Boily, P. L. Gassman, T. Peretyazhko, J. Szanyi and J. M. Zachara, FTIR spectral components of schwertmannite, *Environ. Sci. Technol.*, 2010, **44**, 1185-1190.

54. M. Loan, J. M. Cowley, R. Hart and G. M. Parkinson, Evidence on the structure of synthetic schwertmannite, *Am. Mineral.*, 2004, **89**, 1735-1742.

55. C. Gu, Z. Wang, J. D. Kubicki, X. Wang and M. Zhu, X-ray absorption spectroscopic quantification and speciation modeling of sulfate adsorption on ferrihydrite surfaces, *Environ. Sci. Technol.*, 2016, **50**, 8067-8076.

56. D. Zhang, S. Wang, Y. Wang, M. A. Gomez, Y. Duan and Y. Jia, The transformation of two-line ferrihydrite into crystalline products: effect of pH and media (sulfate versus nitrate), *ACS Earth*

Space Chem., 2018, **2**, 577-587.

57. T. Ishikawa, S. Miyamoto, K. Kandori and T. Nakayama, Influence of anions on the formation of β-FeOOH rusts, *Corros. Sci.*, 2005, **47**, 2510-2520.

58. F. Liu, J. Zhou, S. Zhang, L. Liu, L. Zhou and W. Fan, Schwertmannite synthesis through ferrous ion chemical oxidation under different H_2O_2 supply rates and its removal efficiency for arsenic from contaminated groundwater, *PLoS One*, 2015, **10**, e0138891.

59. A. J. Frierdich, M. Helgeson, C. Liu, C. Wang, K. M. Rosso and M. M. Scherer, Iron atom exchange between hematite and aqueous Fe(II), *Environ. Sci. Technol.*, 2015, **49**, 8479-8486.

60. C. Liu, Z. Zhu, F. Li, T. Liu, C. Liao, J. J. Lee, K. Shih, L. Tao and Y. Wu, Fe(II)-induced phase transformation of ferrihydrite: The inhibition effects and stabilization of divalent metal cations, *Chem. Geol.*, 2016, **444**, 110-119.

61. A. Neumann, L. Wu, W. Li, B. L. Beard, C. M. Johnson, K. M. Rosso, A. J. Frierdich and M. M. Scherer, Atom exchange between aqueous Fe(II) and structural Fe in clay minerals, *Environ. Sci. Technol.*, 2015, **49**, 2786-2795.

62. P. Larese-Casanova, A. Kappler and S. B. Haderlein, Heterogeneous oxidation of Fe(II) on iron oxides in aqueous systems: Identification and controls of Fe(III) product formation, *Geochim. Cosmochim. Acta*, 2012, **91**, 171-186.

63. A. M. Jones, R. N. Collins and T. D. Waite, Redox characterization of the Fe(II)-catalyzed transformation of ferrihydrite to goethite, *Geochim. Cosmochim. Acta*, 2017, **218**, 257-272.

64. V. A. Schoepfer, E. D. Burton and S. G. Johnston, Contrasting effects of phosphate on the rapid transformation of schwertmannite to Fe(III) (oxy)hydroxides at near-neutral pH, *Geoderma*, 2019, **340**, 115-123.

65. K. Sasaki, O. Tanaike and H. Konno, Distinction of jarosie-group compounds by raman spectroscopy, *Can. Mineral.*, 1998, **36**, 1225-1235.

66. F. S. Jones, J. M. Bigham, J. P. Gramp and O. H. Tuovinen, Synthesis and properties of ternary (K, NH_4, H_3O)-jarosites precipitated from Acidithiobacillus ferrooxidans cultures in simulated bioleaching solutions, *Mater. Sci. Eng., C*, 2014, **44**, 391-399.

67. F. S. Jones, J. M. Bigham, J. P. Gramp and O. H. Tuovinen, Formation and characterization of ternary (Na, NH_4, H_3O)-jarosites produced from Acidithiobacillus ferrooxidans cultures, *Appl. Geochem.*, 2018, **91**, 14-22.

68. S. Bai, Z. Xu, M. Wang, Y. Liao, J. Liang, C. Zheng and L. Zhou, Both initial concentrations of Fe(II) and monovalent cations jointly determine the formation of biogenic iron hydroxysulfate precipitates in acidic sulfate-rich environments, *Mater. Sci. Eng., C*, 2012, **32**, 2323-2329.

Figure Captions

Fig. 1. XRD patterns of the products obtained from Fe^{3+} hydrolysis-dialysis at different Fe^{3+} hydrolysis temperatures followed by dialysis for 7 d (a), from Fe^{3+} hydrolysis at 25 and 60 °C followed by dialysis for 1 d and 15 d (b), and from Fe^{3+} hydrolysis at 60 °C in the presence of K^+ or NH_4^+ followed by dialysis for 7 d (c) (Gt = goethite; Sch = schwertmannite).

Fig. 2. SEM images of schwertmannite obtained from Fe^{3+} hydrolysis-dialysis at different Fe^{3+} hydrolysis temperatures followed by dialysis for 7 d (a-25 ºC, b-40 ºC, c-50 ºC, d-60 ºC, e-70 ºC, f-80 ºC) and from different dialysis time at 25 ºC (g-1 d; h-15 d) or at 60 ºC (i-15 d).

Fig. 3. Synchrotron-based XRD patterns (a) and pair distribution functions [G(r)s] (b) of the intermediate products at different aging time after the quickly mixed of a 0.8 M NaOH solution with an equal volume of 0.4 M $Fe_2(SO_4)_3$ and XRD patterns of intermediate products for SO_4^{2-} adsorption on pre-formed ferrihydrite (c) at Fe/S molar ratio of 0.67 and pH 2.5 (Sch = Schwertmannite, Fhy = Ferrihydrite).

Fig. 4. XRD patterns (a) and SEM images (b) of the initial products obtained from direct Fe^{3+} hydrolysis at different Fe^{3+} hydrolysis rates (mixed directly, 33.33, 6.67, and 3.33 μM/min) and pH 3.

Fig. 5. Synchrotron-based XRD patterns and FTIR spectra of the products obtained from direct Fe^{3+} hydrolysis at different Fe^{3+} hydrolysis rates after aging for 3 h (a and c) and 24 h (b and d) at 60 ºC and pH 3 (Gt = goethite; Sch = schwertmannite).

Fig. 6. XRD patterns of the transformation products of schwertmannite, obtained from

Fe^{3+} hydrolysis rate of 6.67 μM/min, at pH 3 and 60 ºC in the presence of Fe^{2+} (a) and the concentrations of dissolved Fe^{2+} and SO_4^{2-} (mM) during the transformation (b) (Fe^{3+}/Fe^{2+} = 10; Gt = goethite; Sch = schwertmannite).

Fig. 7. Concentration of dissolved Fe^{3+} (mM) during the transformation of schwertmannite, obtained from the quick Fe^{3+} hydrolysis (mixed directly), over the pH range of 2.0 - 3.5 (a), Fe/S molar ratios of 1.5 - 10 (b), the temperature range of 25 - 80 ºC (c) and in the presence of Cl^-, K^+ or NH_4^+ (d).

Fig. 8. Concentration of dissolved SO_4^{2-} (mM) during the transformation of schwertmannite, obtained from the quick Fe^{3+} hydrolysis (mixed directly, Fe/S = 2), at different pHs (a), different temperatures (b), in the presence of Cl^- (c) and K^+ or NH_4^+ (d).

Fig. 9. XRD patterns of the mineral phases obtained from quick hydrolysis of Fe^{3+} and SO_4^{2-} (mixed directly) aged for 3 h at different pHs (a), different Fe/S molar ratios (b), different aging temperatures (c) and in the presence of Cl^-, K^+, or NH_4^+ (d) (Gt = goethite; Sch = schwertmannite; Fhy = ferrihydrite; Jt = jarosite).

Fig. 10. SEM images of mineral phases obtained from the quick hydrolysis of Fe^{3+} and SO_4^{2-} (mixed directly) in the presence of Cl^- at 60 °C or in the presence of K^+ or NH_4^+ at 80 °C after aging for 96 h (a: Fe/NH_4^+ = 1; b: Fe/NH_4^+ = 0.1; c: Fe/Cl^- = 0.2; d: Fe/K^+ = 0.1).

Fig. 11. Schematic diagram of schwertmannite formation and transformation through direct Fe^{3+} hydrolysis under various geochemical conditions.

Table 1. The Fe and S contents in the schwertmannite samples formed through Fe^{3+} hydrolysis-dialysis at different hydrolysis temperatures, dialysis time, and in the presence of K^+ or NH_4^+.

Sample	Fe (mmol/g)	SO_4 (mmol/g)	molar ratio of Fe/S
25 °C -7d	10.69	1.71	6.25
40 °C -7d	10.27	1.78	5.77
50 °C -7d	10.65	1.86	5.73
60 °C -7d	10.52	2.03	5.18
70 °C -7d	10.28	1.73	5.94
25 °C -15d	11.55	1.67	6.92
60 °C -15d	11.69	1.79	6.53
60 °C -7d - K^+	9.83	1.66	5.92
60 °C -7d - NH_4^+	11.63	2.13	5.46

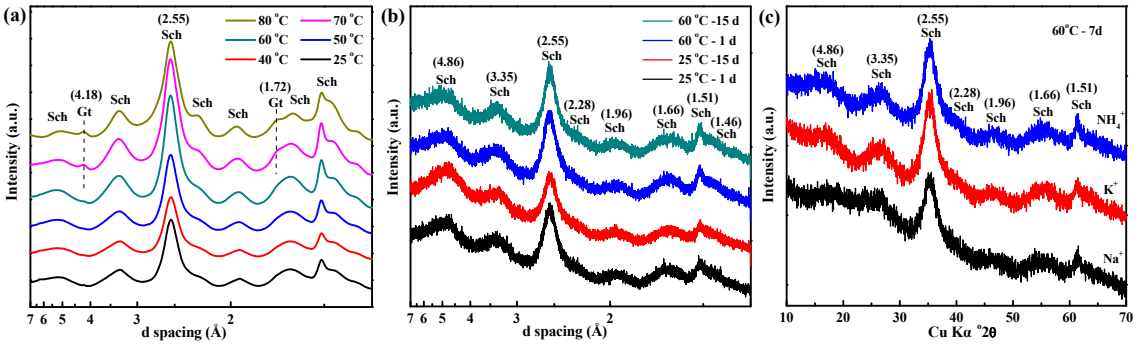

Fig. 1. XRD patterns of the products obtained from Fe^{3+} hydrolysis-dialysis at different Fe^{3+} hydrolysis temperatures followed by dialysis for 7 d (a), from Fe^{3+} hydrolysis at 25 and 60 °C followed by dialysis for 1 d and 15 d (b), and from Fe^{3+} hydrolysis at 60 °C in the presence of K^+ or NH_4^+ followed by dialysis for 7 d (c) (Gt = goethite; Sch = schwertmannite).

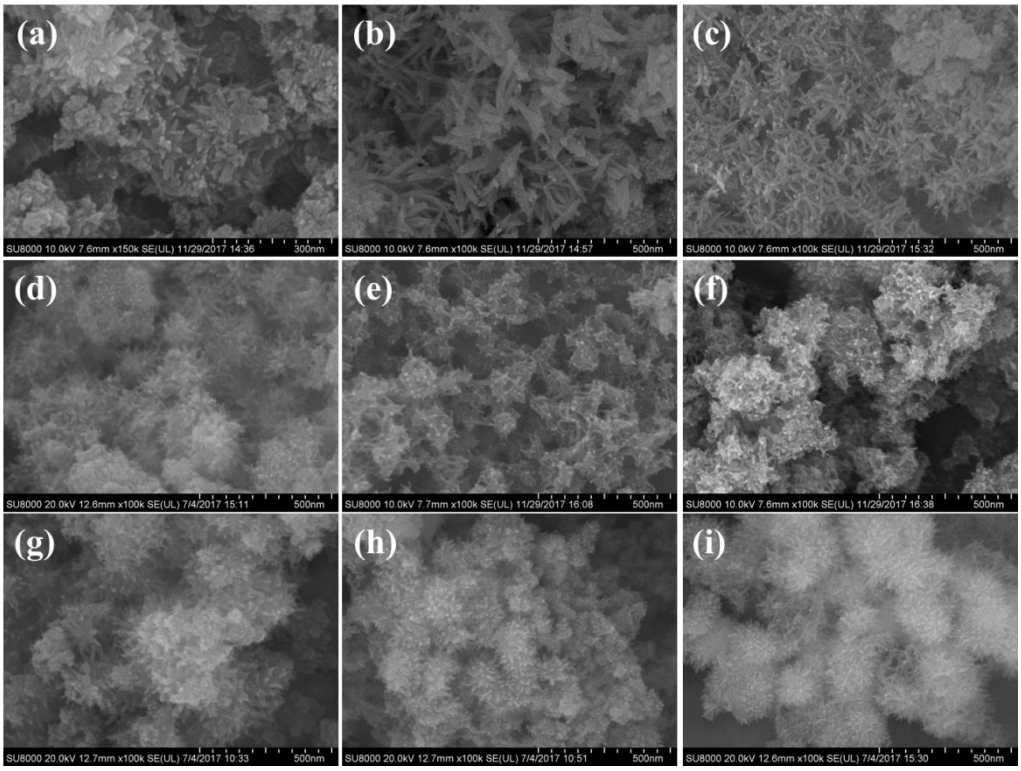

Fig. 2. SEM images of schwertmannite obtained from Fe^{3+} hydrolysis-dialysis at different Fe^{3+} hydrolysis temperatures followed by dialysis for 7 d (a-25 ºC, b-40 ºC, c-50 ºC, d-60 ºC, e-70 ºC, f-80 ºC) and from different dialysis time at 25 ºC (g-1 d; h-15 d) or at 60 ºC (i-15 d).

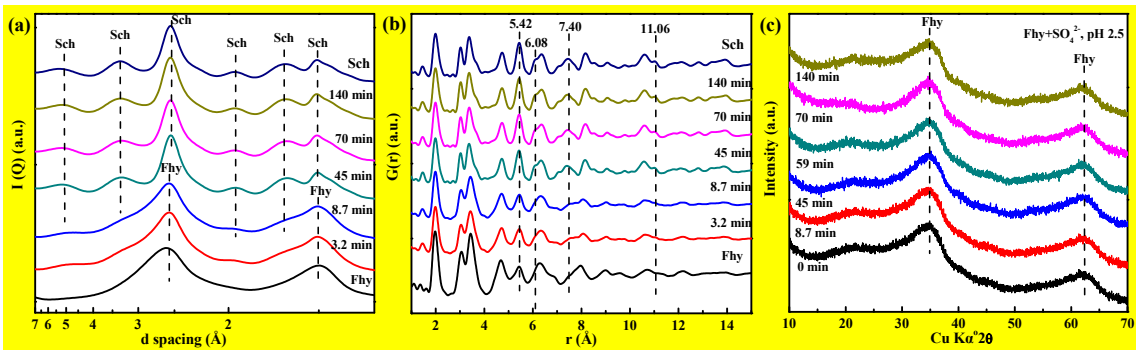

Fig. 3. Synchrotron-based XRD patterns (a) and pair distribution functions [G(r)s] (b) of the intermediate products at different aging time after the quickly mixed of a 0.8 M NaOH solution with an equal volume of 0.4 M $Fe_2(SO_4)_3$ and XRD patterns of intermediate products for SO_4^{2-} adsorption on pre-formed ferrihydrite (c) at Fe/S molar ratio of 0.67 and pH 2.5 (Sch = Schwertmannite, Fhy = Ferrihydrite).

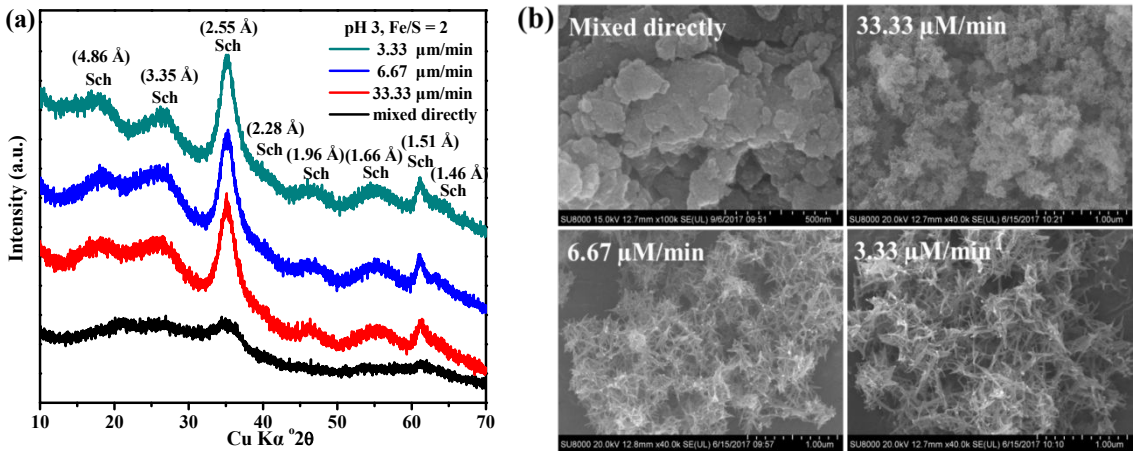

Fig. 4. XRD patterns (a) and SEM images (b) of the initial products obtained from direct Fe^{3+} hydrolysis at different Fe^{3+} hydrolysis rates (mixed directly, 33.33, 6.67, and 3.33 μM/min) and pH 3.

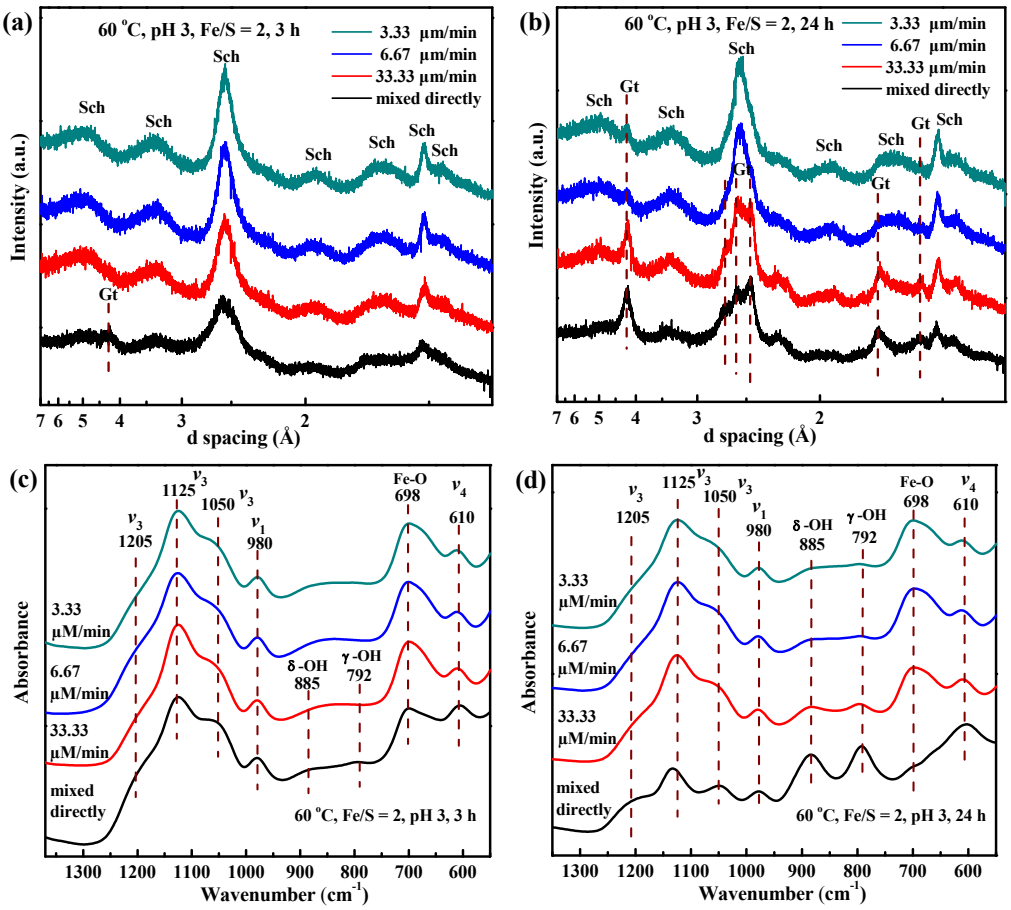

Fig. 5. Synchrotron-based XRD patterns and FTIR spectra of the products obtained from direct Fe^{3+} hydrolysis at different Fe^{3+} hydrolysis rates after aging for 3 h (a and c) and 24 h (b and d) at 60 ºC and pH 3 (Gt = goethite; Sch = schwertmannite).

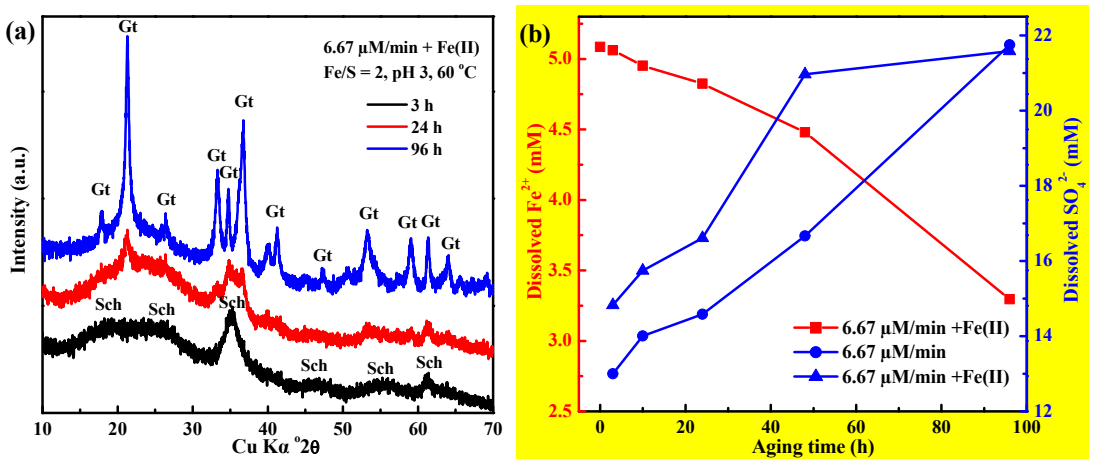

Fig. 6. XRD patterns of the transformation products of schwertmannite, obtained from Fe^{3+} hydrolysis rate of 6.67 µM/min, at pH 3 and 60 ºC in the presence of Fe^{2+} (a) and the concentrations of dissolved Fe^{2+} and SO_4^{2-} (mM) during the transformation (b) ($Fe^{3+}/Fe^{2+} = 10$; Gt = goethite; Sch = schwertmannite).

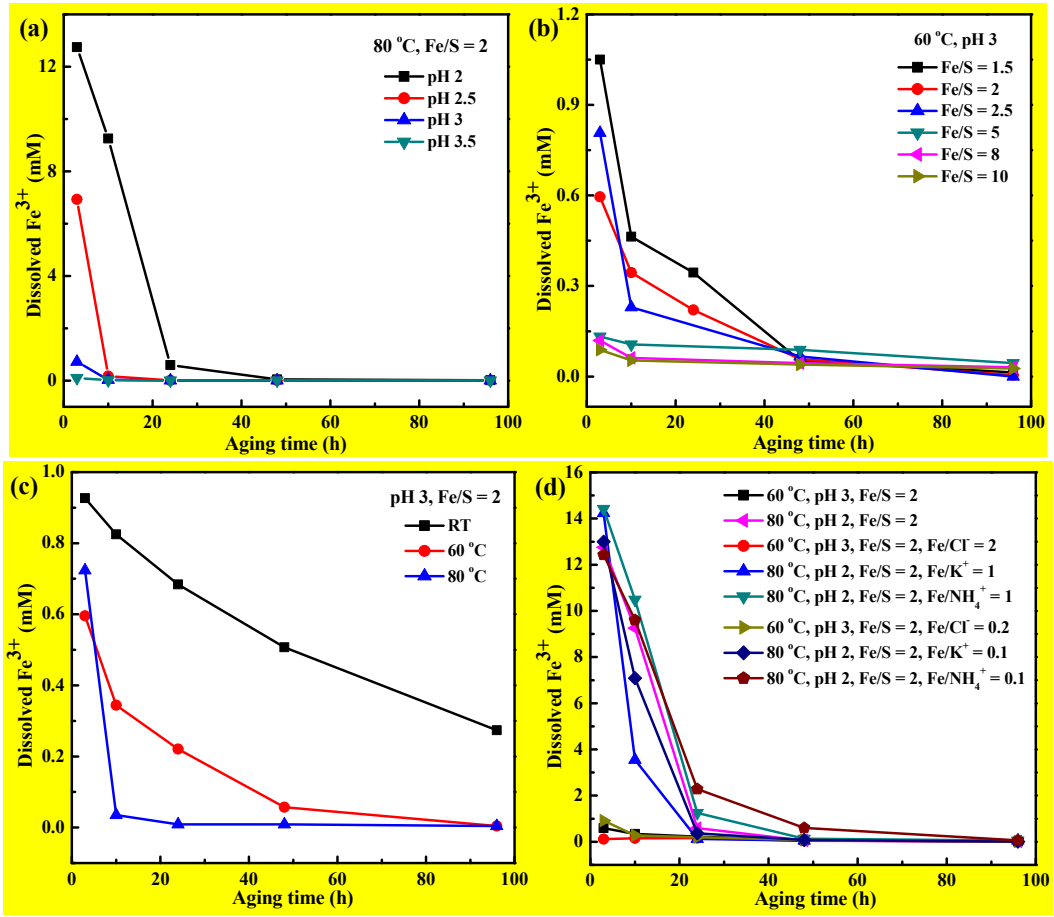

Fig. 7. Concentration of dissolved Fe^{3+} (mM) during the transformation of schwertmannite, obtained from the quick Fe^{3+} hydrolysis (mixed directly), over the pH range of 2.0 - 3.5 (a), Fe/S molar ratios of 1.5 - 10 (b), the temperature range of 25 - 80 ^{o}C (c) and in the presence of Cl^{-}, K^{+} or NH_4^{+} (d).

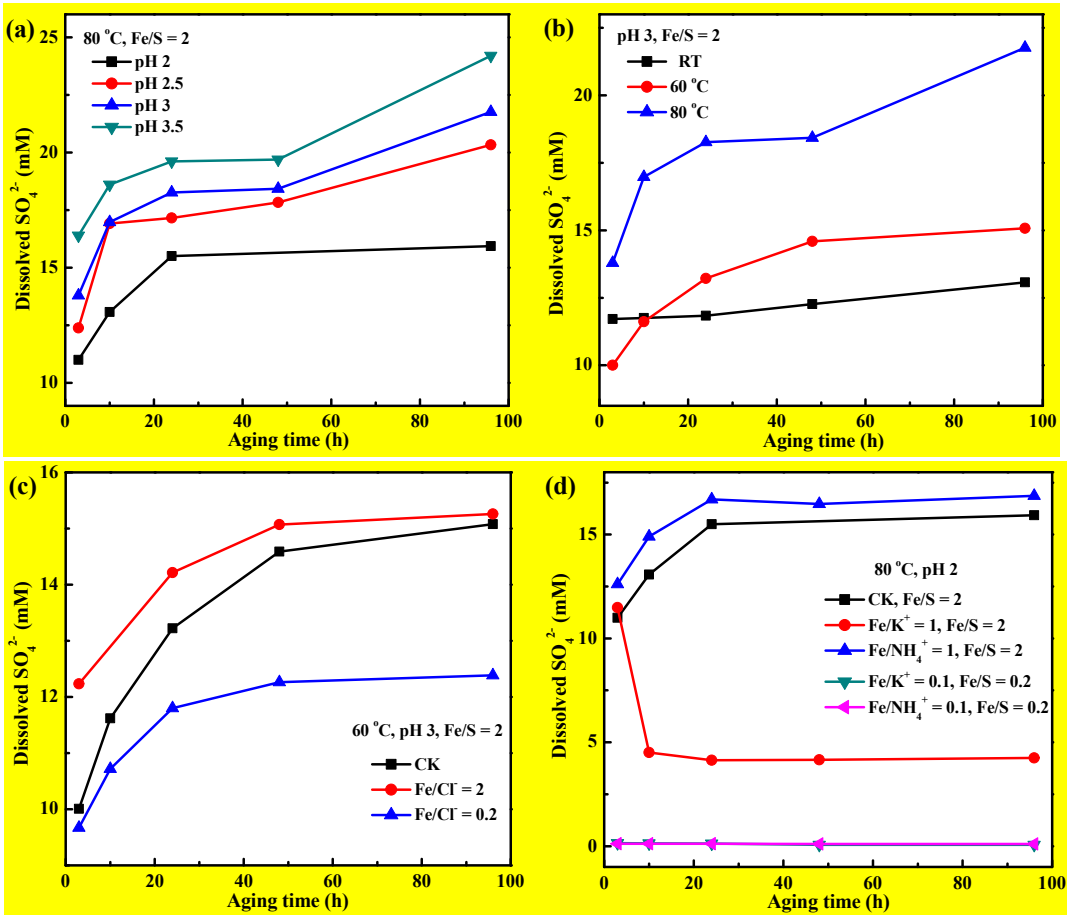

Fig. 8. Concentration of dissolved SO_4^{2-} (mM) during the transformation of schwertmannite, obtained from the quick Fe^{3+} hydrolysis (mixed directly), at different pHs (a), different temperatures (b), in the presence of Cl^- (c) and K^+ or NH_4^+ (d).

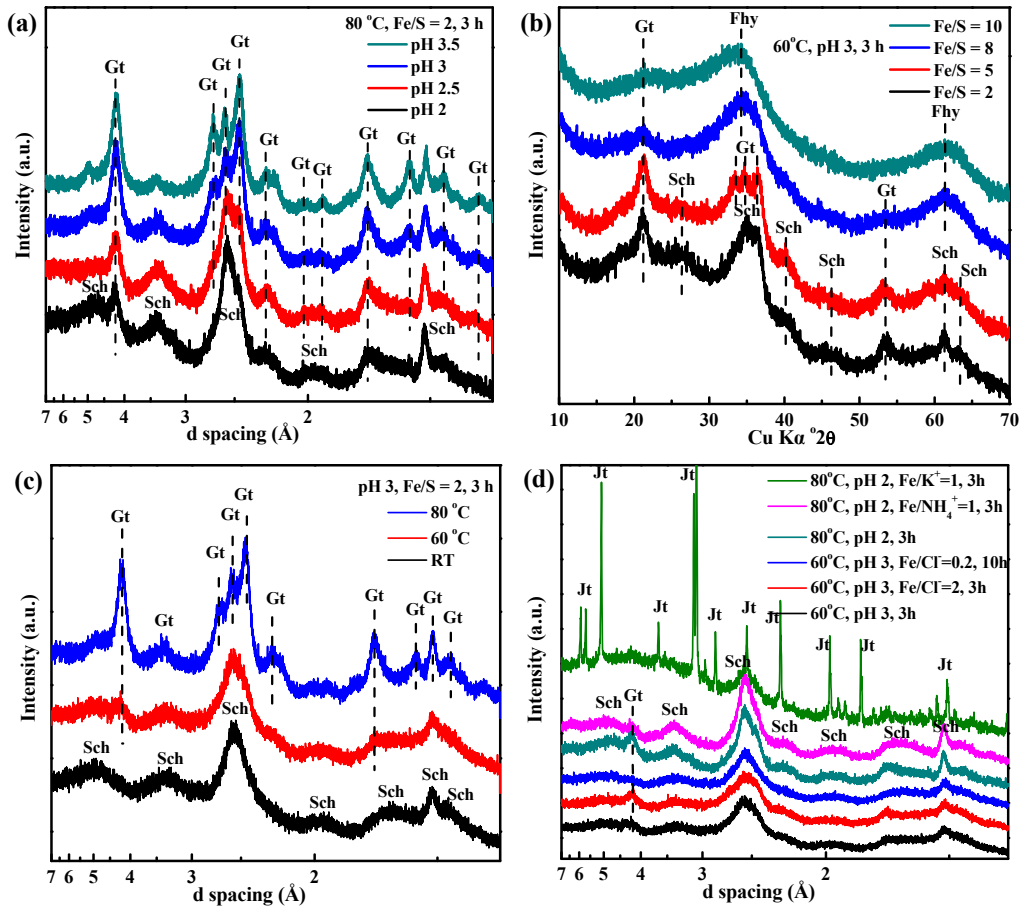

Fig. 9. XRD patterns of the mineral phases obtained from quick hydrolysis of Fe^{3+} and SO_4^{2-} (mixed directly) aged for 3 h at different pHs (a), different Fe/S molar ratios (b), different aging temperatures (c) and in the presence of Cl^-, K^+, or NH_4^+ (d) (Gt = goethite; Sch = schwertmannite; Fhy = ferrihydrite; Jt = jarosite).

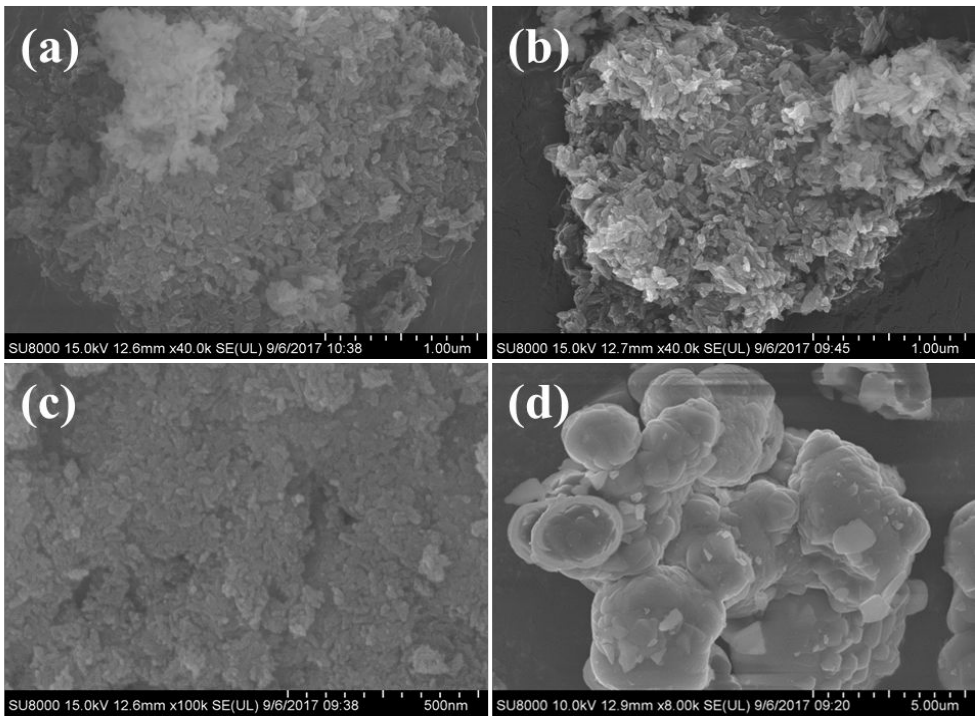

Fig. 10. SEM images of mineral phases obtained from the quick hydrolysis of Fe^{3+} and SO_4^{2-} (mixed directly) in the presence of Cl^- at 60 °C or in the presence of K^+ or NH_4^+ at 80 °C after aging for 96 h (a: $Fe/NH_4^+ = 1$; b: $Fe/NH_4^+ = 0.1$; c: $Fe/Cl^- = 0.2$; d: $Fe/K^+ = 0.1$).

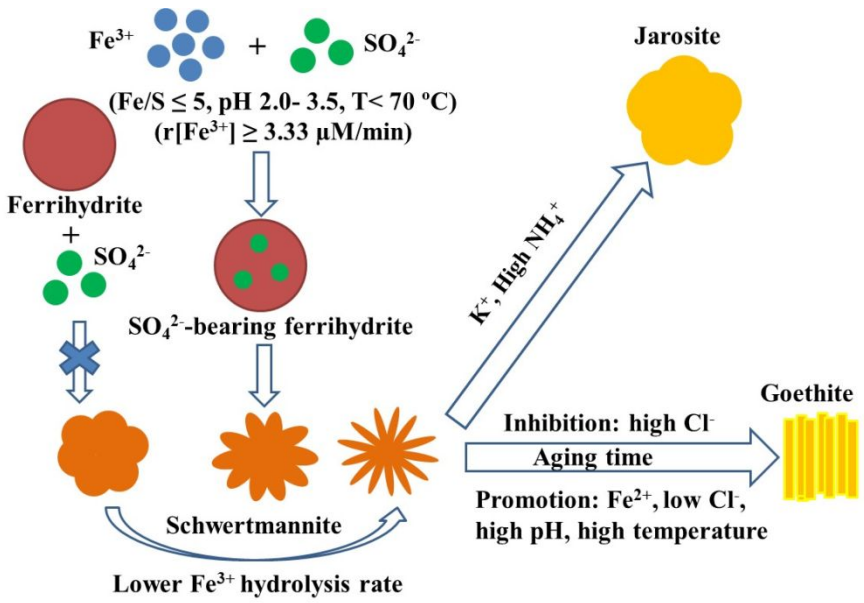

739

740 **Fig. 11.** Schematic diagram of schwertmannite formation and transformation through

741 direct Fe^{3+} hydrolysis under various geochemical conditions.

742

Electronic supplementary information

Formation and transformation of schwertmannite through direct Fe^{3+} hydrolysis under various geochemical conditions

Hong Ying[a], Xionghan Feng[a], Mengqiang Zhu[b], Bruno Lanson[c], Fan Liu[a], Xiaoming Wang[a,*]

[a] Key Laboratory of Arable Land Conservation (Middle and Lower Reaches of Yangtze River), Ministry of Agriculture, College of Resources and Environment, Huazhong Agricultural University, Wuhan 430070, China

[b] Department of Ecosystem Science and Management, University of Wyoming, Laramie, WY, 82071

[c] Univ. Grenoble Alpes, Univ. Savoie-Mont Blanc, CNRS, IRD, IFSTTAR, ISTerre, F-38000 Grenoble, France

Supplementary data includes 1 table and 5 figures.

*Corresponding author:

Xiaoming Wang, Tel: +86 27 87280271; Fax: +86 27 87288618; E-mail: wangxm338@mail.hzau.edu.cn

Table S1. Experimental conditions on formation and transformation of schwertmannite through direct Fe^{3+} hydrolysis

Sample	Fe^{3+} (mM)	SO_4^{2-} (mM)	pH	Temperature	Co-existing ions (mM)	Dialysis time
(a) Schwertmannite formation though Fe^{3+} hydrolysis-dialysis pathway						
Hydrolysis temperature	19.98	10.56	-	25, 40, 50, 60, 70, 80 °C	-	7d
Dialysis time	19.98	10.56	-	25, 60 °C	-	1, 3, 7, 15 d
Coexistence of K^+ or NH_4^+	19.98	10.56	-	60 °C	K^+, NH_4^+ (21.12 mM)	7d
(b) Mineral evolution during Fe^{3+} hydrolysis by adding NaOH						
OH^-/Fe^{3+} = 1	400	600	2.5	25 °C	-	-
Fhy + SO_4^{2-}	48.55	72.825	2.5	25 °C	-	-
(c) Fe^{3+} hydrolysis rate on the formation and long-term aging of schwertmannite						
33.33 μM/min	48.55	24.275	3.0	Formed:25 °C Aging: 60 °C	-	-
6.67 μM/min	48.55	24.275	3.0	Formed:25 °C Aging: 60 °C	-	-
3.33 μM/min	48.55	24.275	3.0	Formed:25 °C Aging: 60 °C	-	-
(d) Schwertmannite transformation under various geochemical conditions						
pH effects	48.55	24.275	2.0, 2.5, 3.0, 3.5	Aging: 80 °C	-	-
Fe/S molar ratios	48.55	32.37, 24.275, 19.42, 9.71, 6.07, 4.855	3.0	Aging: 60 °C	-	-

Aging temperature	48.55	24.275	3.0	25, 60, 80 °C	-	-
Co-existing Fe^{2+}	48.55	24.275	3.0	Aging: 60 °C	Fe^{2+} (4.855 mM)	-
Co-existing Cl^-	48.55	24.274	3.0	Aging: 60 °C	Cl^- (24.275, 242.75 mM)	-
Co-existing K^+ or NH_4^+	48.55	24.275, 247.25	2.0	Aging: 80 °C	K^+, NH_4^+ (48.55, 485.5 mM)	-

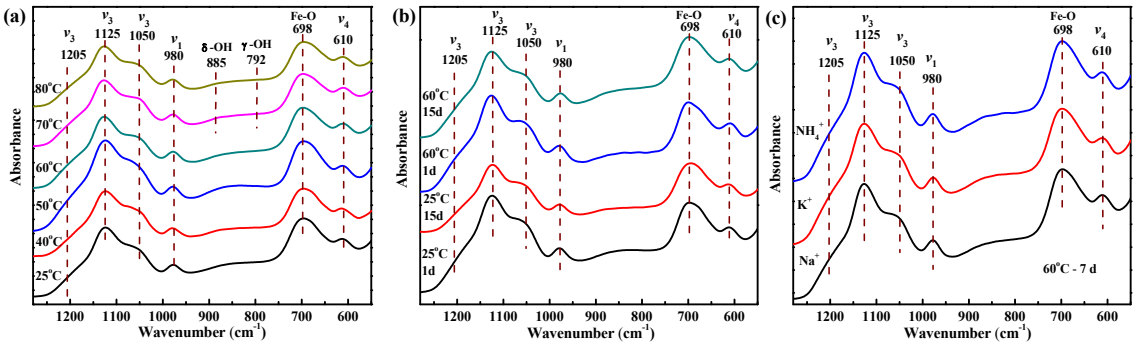

Fig. S1. FTIR spectra of the products obtained from Fe^{3+} hydrolysis-dialysis at different Fe^{3+} hydrolysis temperatures followed by dialysis for 7 d (a), from Fe^{3+} hydrolysis at 25 °C and 60 °C followed by dialysis for 1 d and 15 d (b), and from Fe^{3+} hydrolysis at 60 °C in the presence of K^+ or NH_4^+ followed by dialysis for 7 d (c).

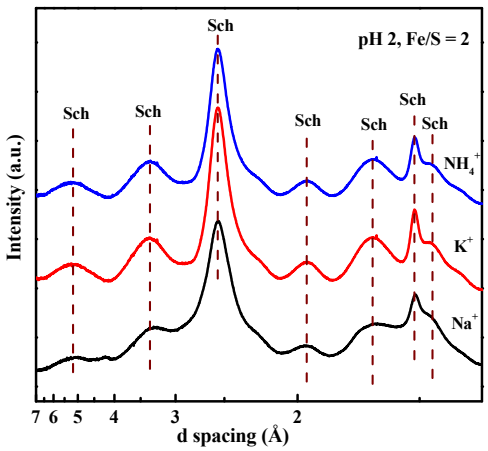

Fig. S2. Synchrotron based XRD patterns of the products obtained from quick

hydrolysis of Fe^{3+} and SO_4^{2-} (mixed directly) in the presence of K^+ or NH_4^+ (Fe/S = 2, Fe/ K^+ or NH_4^+ = 1) at pH 2 and 25 °C (Sch = schwertmannite).

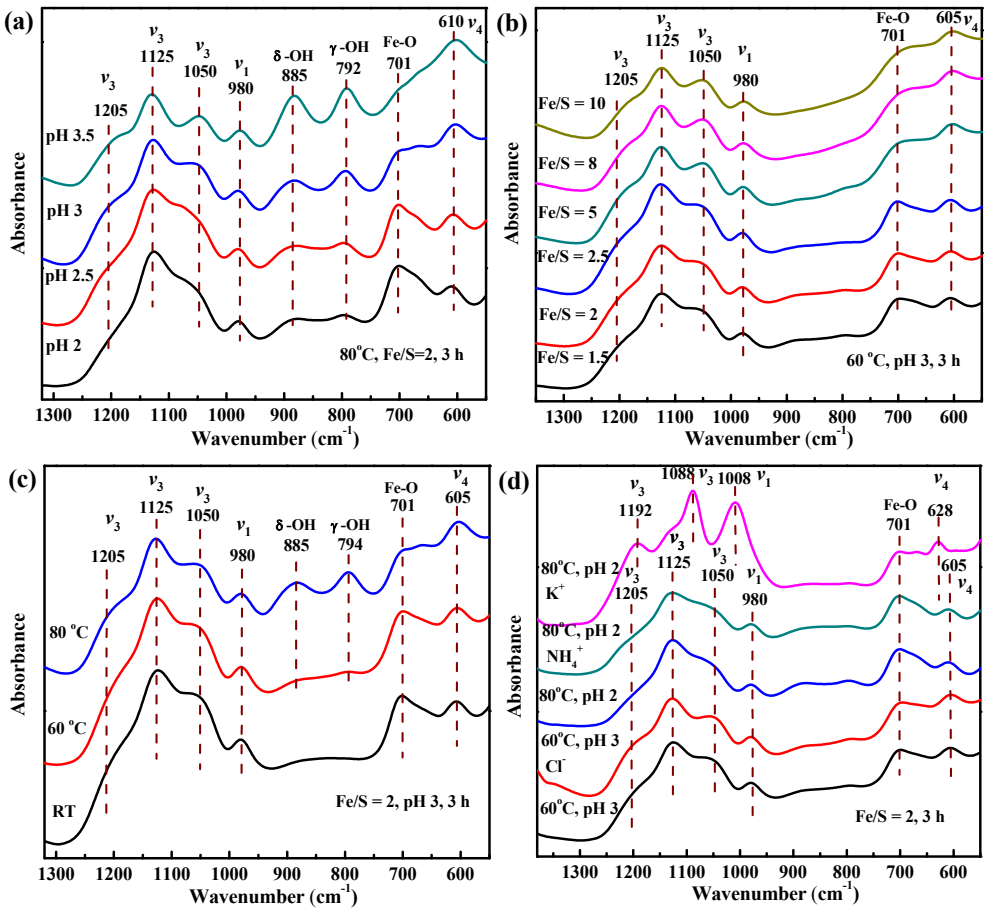

Fig. S3. FTIR spectra of the mineral phases obtained from quick hydrolysis of Fe^{3+} and SO_4^{2-} (mixed directly) aged for 3 h at different pHs (a), different Fe/S molar ratios (b), different aging temperatures (c) and in the presence of Cl^-, K^+ or NH_4^+ (d).

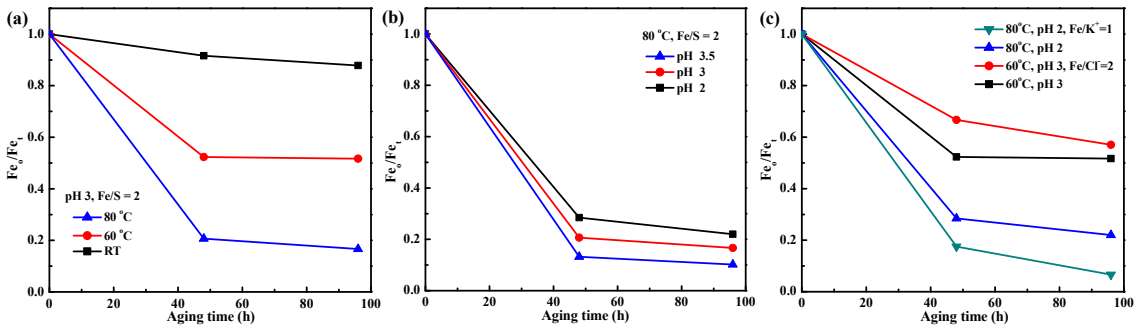

Fig. S4. The transformation rate described as Fe_o/Fe_t of schwertmannite obtained from quick hydrolysis of Fe^{3+} and SO_4^{2-} (mixed directly) during aging at different temperatures (a), at different pHs (b) and in the presence of Cl^- or K^+ (c) (Fe_o: weak crystalline iron, dissolved by 0.2 M acidic ammonium oxalate; Fe_t: total iron, dissolved by 4 M HCl).

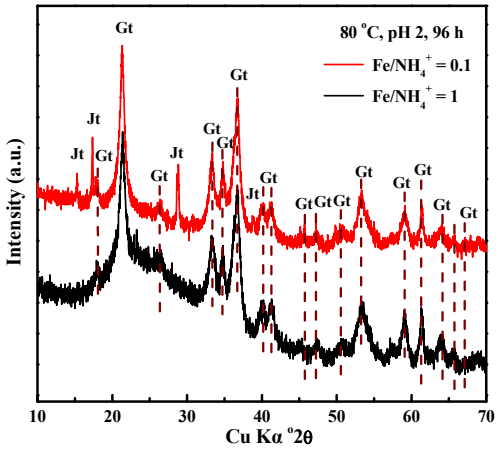

Fig. S5. XRD patterns of the mineral phases obtained from quick hydrolysis of Fe^{3+} and SO_4^{2-} (mixed directly) in the presence of NH_4^+ (Fe/NH_4^+ = 0.1 or 1) at 80 °C and pH 2 after aging for 96 h (Gt = goethite, Jt = jarosite).